

## Finite element modeling of surge propagation and an application to the Hay River, N.W.T.

F. E. HICKS, P. M. STEFFLER, AND R. GERARD

*Department of Civil Engineering, University of Alberta, Edmonton, Alta., Canada T6G 2G7*

Received May 13, 1991

Revised manuscript accepted November 5, 1991

This paper describes the application of the characteristic-dissipative-Galerkin method to steady and unsteady open channel flow problems. The robust performance of this new finite element scheme is demonstrated in modeling the propagation of ice jam release surges over a 500 km reach of the Hay River in Alberta and Northwest Territories. This demonstration includes the automatic determination of steady flow profiles through supercritical-subcritical transitions, establishing the initial conditions for the unsteady flow analyses. The ice jam releases create a dambreak type of problem which begins as a very dynamic situation then develops into an essentially kinematic wave problem as the disturbance propagated downstream. The characteristic-dissipative-Galerkin scheme provided stable solutions not only for the extremes of dynamic and kinematic wave conditions, but also through the transition between the two.

*Key words:* open channel flow, finite element method, dam break, surge propagation.

Cet article décrit l'application de la méthode de Galerkin aux problèmes d'écoulements permanent et non permanent à surface libre. La performance de cette nouvelle méthode des éléments finis est démontrée en modélisant la propagation d'une débâcle sur la rivière Hay, en Alberta et dans les Territoires du Nord-Ouest sur une distance de 500 km. Cette démonstration comprend la détermination automatique des profils d'écoulement permanent par des transitions torrentielle/fluviale, permettant d'établir les conditions initiales des analyses de l'écoulement non permanent. Les débâcles créent un type de problème qui au départ constitue une situation très dynamique pour se transformer ensuite essentiellement en problème de vague cinématique au fur et à mesure que la perturbation se propage en aval. La méthode de Galerkin a permis d'élaborer des solutions stables non seulement pour les conditions extrêmes (vague dynamique et vague cinématique), mais aussi pour la transition entre les deux.

*Mots clés :* écoulement à surface libre, méthode des éléments finis, débâcle, propagation des surpressions.

[Traduit par la rédaction]

Can. J. Civ. Eng. 19, 454-462 (1992)

### Introduction

The understanding and prediction of the behavior of flow in open channels is important to the solution of a wide variety of practical flow problems in water resources engineering. For example, flood forecasting and floodplain delineation; the design of flood protection works, culverts, spillways and diversion canals; and the assessment of the impact of dam failure or a sudden ice jam release, all require knowledge of the water surface elevation, discharge, and velocity in an open channel. However, even if the flow is approximated as one-dimensional, the governing nonlinear system of partial differential equations describing these problems may be difficult to solve, particularly in cases where the flow may be either subcritical or supercritical or a combination of both. Typically, reach subdivision by trial and error is required to compute the unique solution. Solutions may also be obtained for simplified cases by neglecting certain terms in the equations. For example, the flow may be approximated by a kinematic or diffusive wave. Unfortunately, these solutions are restricted in their applicability and more than one flow approximation may be required within the domain of concern. However, as a result of a comprehensive examination of the state of the art in finite element modeling of open channel flow, a new approach entitled the characteristic-dissipative-Galerkin (CDG) scheme has recently been developed (Hicks and

Steffler 1992), which overcomes many of these limitations and which has been shown to provide accurate and stable solutions to a wide variety of open channel flow problems (Hicks and Steffler 1990; 1992).

This paper illustrates the robust performance of the CDG method in practical situations, by applying it to the determination of the propagation of ice jam release surges over a 500 km reach of the Hay River in Alberta and Northwest Territories. As described below, this reach is characterized by a large range of slopes resulting in supercritical-subcritical transitions which were captured without special treatment or subdivision by the CDG method. This application is also significant in that the surges created by the ice jam release begin as very dynamic waves and then develop into essentially kinematic waves as the disturbance propagates downstream. The CDG scheme provided stable solutions not only for the extremes of the dynamic and kinematic wave conditions, but through the transition between the two as well. This unsteady model may also be applied to the solution of steady flow problems, in which case the time step acts as an underrelaxation factor in the iteration, thereby allowing hydraulic jumps to develop and position in a controlled fashion.

### Characteristic-dissipative-Galerkin method formulation

#### *One-dimensional equations of unsteady open channel flow*

The St. Venant equations describe conservation of mass and momentum for one-dimensional, unsteady flow in an open channel. Neglecting lateral inflow, they may be written as

NOTE: Written discussion of this paper is welcomed and will be received by the Editor until October 31, 1992 (address inside front cover).

$$[1] \quad \frac{\partial\{\phi\}}{\partial t} + \frac{\partial\{F\}}{\partial x} + \{f_c\} = \{0\}$$

where

$$\{\phi\} \equiv \begin{Bmatrix} A \\ Q \end{Bmatrix}$$

$$[2] \quad \{F\} \equiv \begin{Bmatrix} Q \\ UQ + \frac{gAH}{2} \end{Bmatrix}$$

$$\{f_c\} \equiv \begin{Bmatrix} 0 \\ -gA \left( S_0 + \frac{H}{2B} \frac{dB}{dx} - S_f \right) \end{Bmatrix}$$

where  $A$  represents the flow area;  $B$ , the channel width;  $Q$ , the discharge;  $U$ , the cross-sectionally averaged longitudinal velocity;  $S_0$ , the longitudinal bed slope;  $S_f$ , the longitudinal friction slope;  $g$ , the acceleration due to gravity; and  $x$  and  $t$ , the longitudinal distance and temporal coordinates, respectively.

For this study, the friction slope was evaluated based on Chezy's equation,

$$[3] \quad U = C_* \sqrt{gRS_f}$$

where  $C_*$  is the non-dimensional Chezy coefficient (Henderson 1966) and  $R$  is the hydraulic radius, which is equal to the area divided by the wetted perimeter,

$$[4] \quad R = \frac{A}{P}$$

The coefficient  $C_*$  was determined based on the log-law (Schlichting 1979):

$$[5] \quad C_* = 5.75 \log \left( \frac{R}{k} \right) + K$$

where  $k$  is the effective channel roughness (Schlichting 1979) and  $K$  is a constant. Based on experiments and theoretical analysis, values of  $K$  for pipe flow of 6.6 and 6.5 have been determined (Keulegan 1938), respectively. A theoretical value of 6.0 has been determined for the flow between two infinite parallel plates (Keulegan 1938; White 1986). Based on these, an intermediate value of  $K = 6.2$  was considered appropriate for an open channel, for this study.

An alternative approach for evaluating the friction slope is to use Manning's equation (Chow 1959),

$$[6] \quad U = \frac{R^{2/3} S_f^{1/2}}{n}$$

(for SI units) where  $n$  is the Manning coefficient.

When an ice cover is present, the resistance force is evaluated by increasing the wetted perimeter to include the water surface area on which the ice floats. In addition, a composite effective roughness is determined, which incorporates the resistance effects on both the bed and the underside of the ice cover. This is discussed further in the section on the ice jam simulation.

### Finite element implementation

Equations [1] and [2] are a system of nonlinear partial differential equations which may be solved by a number of

numerical methods, generally classified as either finite difference methods or finite element methods. Of the finite difference models, the four-point implicit ("box") scheme as presented by Amien (1968) has been used most frequently to solve these equations and, for example, forms the basis of the familiar DAMBRK code (Fread 1988). However, the underlying consistency and generality of the finite element method provides a number of advantages over the finite difference approach. One of the most restrictive limitations of finite difference methods is that they require separate computational algorithms for subcritical and supercritical flows. Therefore, should supercritical flow occur locally in some reaches, as in the Hay River case, subcritical and supercritical flows must be modeled separately and then the final solutions of each reach pieced together. In contrast, the finite element method handles subcritical and supercritical flows in the same way, thereby enabling it to solve for both flow regimes simultaneously.

In this study, the finite element equations were derived using the Galerkin weighted residual method. The simplest implementation, commonly known as the Bubnov-Galerkin method (analogous to centered finite differences), is useful for modeling relatively flat waves, but it performs poorly in the vicinity of steep gradients in the solution because oscillations occur and the solution deteriorates rapidly (Katapodes 1984; Hicks and Steffler 1990). In this study, researches into finite element methods for open channel flow applications, particularly the dissipative-Galerkin scheme of Katopodes (1984) and the work of Hughes and Mallet (1986), lead to the development of a new finite element model, the characteristic-dissipative-Galerkin (CDG) method which has the ability to provide numerically stable solutions. This improvement is achieved through the use of upwind weighted test functions which introduce selective artificial dissipation, smoothing out spurious, short wavelength, oscillations. Essentially, this is equivalent to a Bubnov-Galerkin formulation of the extended system,

$$[7] \quad \left( \frac{\partial\{\phi\}}{\partial t} + \frac{\partial\{F\}}{\partial x} + \{f_c\} \right) - \omega \frac{\Delta x}{2} \frac{[A]}{|[A]|} \frac{\partial}{\partial x} \left( \frac{\partial\{\phi\}}{\partial t} + [A] \frac{\partial\{\phi\}}{\partial x} + \{f_n\} \right) = \{0\}$$

(original system) (upwinding terms)

where

$$[8] \quad [A] \equiv \frac{\partial\{F\}}{\partial\{\phi\}} = \begin{bmatrix} 0 & 1 \\ c^2 - U^2 & 2U \end{bmatrix}$$

and

$$[9] \quad \{f\} \equiv \begin{Bmatrix} 0 \\ -gA \left( S_0 + \frac{H}{B} \frac{dB}{dx} - S_f \right) \end{Bmatrix}$$

and in which

$$[10] \quad c \equiv \sqrt{gH}$$

is the celerity of a small gravity wave and  $\Delta x$  is the element length. A constant value of 0.25 for the upwinding parameter,  $\omega$ , minimizes dissipation of long wavelengths (com-

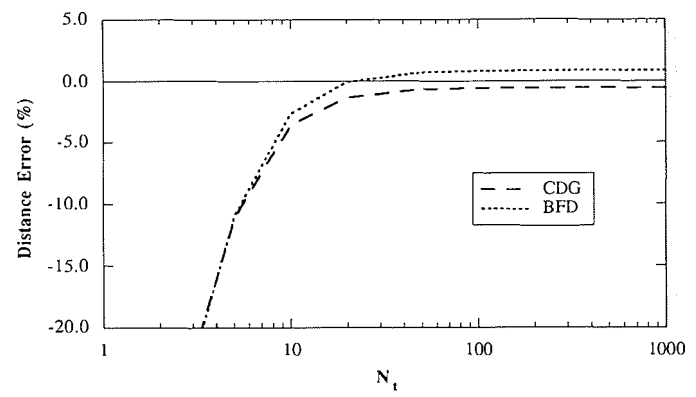
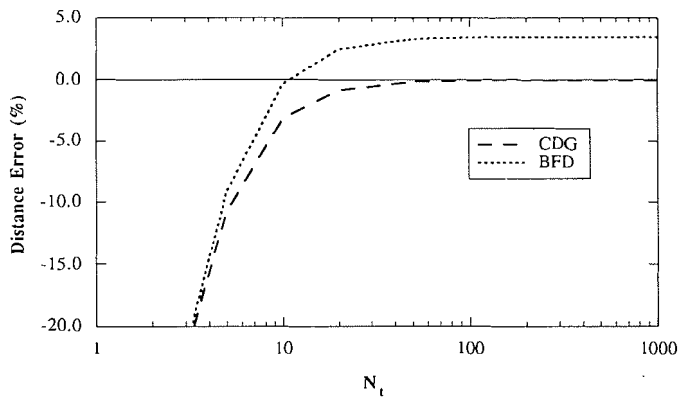
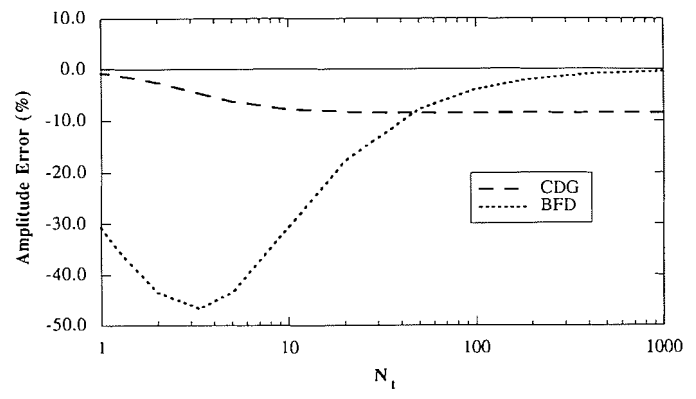
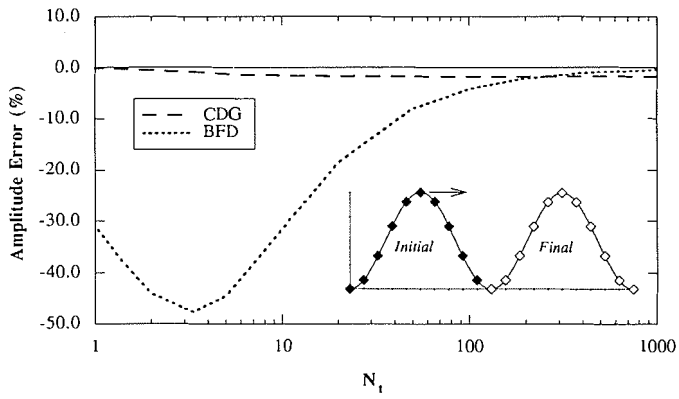


FIG. 1. Comparison of the amplitude and distance errors of the CDG ( $\theta = 0.5$ ) and BFD ( $\theta = 0.6$ ) methods as a function of the temporal discretization (progressive waves, after propagating one wavelength; resolution: 10 nodes per wavelength).

FIG. 2. Comparison of the amplitude and distance errors of the CDG ( $\theta = 0.5$ ; resolution: 6 nodes per wavelength) and BFD ( $\theta = 0.6$ ; resolution: 20 nodes per wavelength) methods as a function of the temporal discretization (progressive waves, after propagating one wavelength).

pared to  $\Delta x$ ) while achieving good phase accuracy (Hicks and Steffler 1990) while the coefficient matrix

$$[11] \frac{[A]}{[A]} = \begin{bmatrix} \frac{1}{2c} & -\frac{1}{2c} \\ \frac{U+c}{2c} & \frac{U-c}{2c} \end{bmatrix} \begin{bmatrix} \frac{U+c}{|U+c|} & 0 \\ 0 & \frac{U-c}{|U-c|} \end{bmatrix} \begin{bmatrix} -(U-c) & 1 \\ -(U+c) & 1 \end{bmatrix}$$

controls the distribution of the upwinding. It should be noted that phase accuracy may be optimized by employing a value of  $\omega = 0.5$ , with slightly increased dissipation. However, the effect on phase and amplitude is only marginal.

It may also be noted that the upwinding terms are formed from derivatives of the non-conservation form of the original system. Artificial dissipation is introduced through the second derivative in  $x$ , and is balanced to third order by the other upwinding terms (Baker 1983) when a semi-implicit formulation is used. Defining the implicitness factor as  $\theta$ , this process corresponds to  $\theta = 0.5$ .

*Linear Fourier analysis*

The amplification and phase characteristics of the CDG scheme for the linearized St. Venant equations have been

examined through Fourier analysis and compared to the box finite difference (BFD) scheme (Hicks and Steffler 1990). Although such an analysis cannot predict instabilities associated with nonlinearities in the problem, it is a valuable tool as a basis for the comparison of various numerical schemes and also helps to determine the appropriate discretization of a problem for a particular method. Using this approach the CDG scheme was found to be particularly successful at selectively damping the high frequency wavelengths associated with numerical instabilities, while maintaining good phase accuracy (Hicks and Steffler 1990).

To illustrate the relative performance of the BFD and CDG schemes, Fig. 1 shows the results of the linear stability analysis for a spatial discretization of 10 nodes per wavelength. In this figure, the amplitude and distance errors, defined as the difference between the numerical and exact values divided by the exact values, have been determined for the propagation of a purely dynamic wave (neglecting slope and friction) for one wavelength and are presented as a function of the number of time steps,  $N_t$ , used in propagating the disturbance this distance. Here, the BFD scheme has been analyzed at the implicitness  $\theta = 0.6$  recommended by Fread (1988). As the figure shows, the speed of the disturbance would be predicted exactly using the BFD scheme at  $N_t = 10$  (corresponding to a Courant number,  $(U + c)\Delta t/\Delta x = 1$ ). However, the amplitude of the wave would be decreased by about 30% for each wavelength travelled. If an attempt was made to reduce the amplitude error by using more time steps, a phase speed error would be introduced, resulting

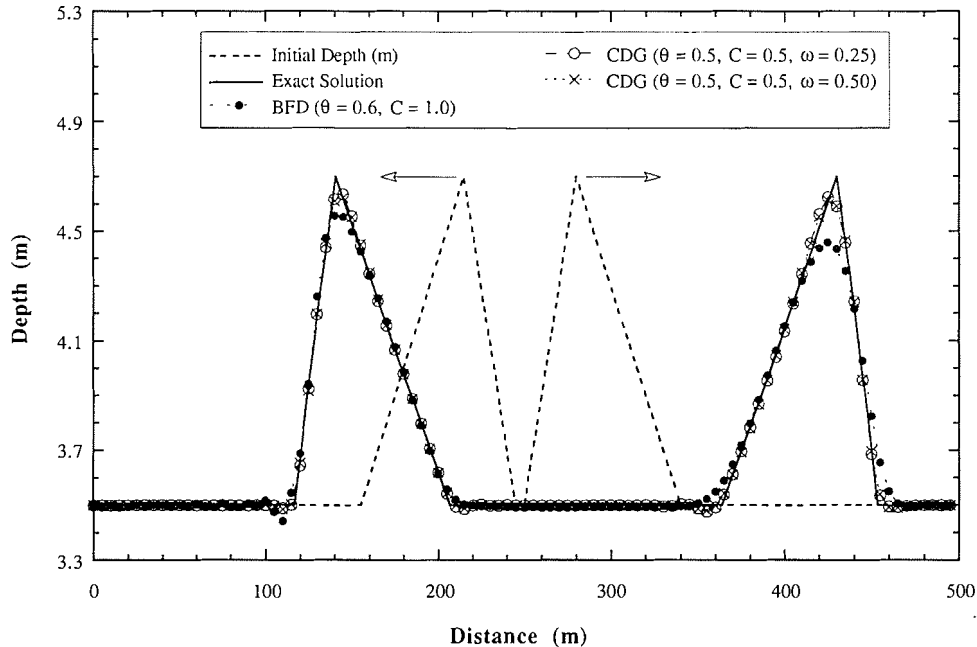


FIG. 3. Comparison of the CDG and BFD schemes for the propagation of progressive and regressive disturbances.

in wave dispersion. Small phase errors can result in severe apparent oscillations as waves of differing wavelengths are propagated at slightly different speeds. In contrast, the CDG scheme is capable of achieving good distance and amplitude accuracy with  $N_t$  greater than or equal to about 20.

The BFD scheme was also found to require a node density of 2 to 3 times that required by the CDG scheme in order to achieve comparable accuracy. This is illustrated in Fig. 2, which shows a situation in which comparable phase accuracy is achieved for the two schemes. It can be seen that, for this same level of accuracy, the CDG scheme requires a resolution of only 6 nodes per wavelength while the BFD method requires a resolution of 20 nodes per wavelength, which is three times larger than the CDG scheme. Although the BFD scheme demonstrates zero distance error at  $N_t = 20$ , the amplitude error at this temporal discretization would be of the order of 20%. In addition, since the  $N_t$  required to achieve exact phase speed depends on the spatial discretization, nonlinear disturbances (which may be considered to be comprised of a number of components of varying wavelength) would achieve exact phase speed accuracy for only one component. Therefore, dispersion effects can be expected in any nonlinear problem. The CDG scheme exhibits comparable phase accuracy, but the amplitude error remains relatively constant at about 8% for  $N_t$  values greater than 10.

These predictions of the linear stability analysis have been confirmed through extensive nonlinear numerical simulations over a wide range of flow conditions (Hicks and Steffler 1990, 1992). Specifically, the tests included disturbance propagation in subcritical and supercritical flows, dam break tests, and the propagation of waves through hydraulic jumps. Friction-dominated diffusive and kinematic wave propagation situations were also tested.

To illustrate the comparative accuracy of the BFD and CDG schemes in propagating disturbances, the results for one of the tests are presented here. By eliminating the friction and slope terms from consideration, exact solutions

based on the method of characteristics could be obtained easily, thus facilitating this evaluation. The geometry consisted of a unit-width section of a horizontal, frictionless channel discretized into 99 elements, each 5 m long. To facilitate the computation of exact solutions for this nonlinear problem, the initial conditions were set as two identical disturbances, one progressive and one regressive. Throughout the simulation, discharge was the condition specified at the upstream and downstream boundaries. The initial depth was taken as 3.5 m, except in the vicinity of the two disturbances. The initial discharge was specified based upon the Froude number,  $F$ , chosen for the undisturbed flow, where

$$[12] \quad F = \frac{U}{c}$$

Figure 3 illustrates the initial depth condition specified for this test, which corresponds to  $F = 0.5$  in the undisturbed flow (flow is from left to right). The CDG scheme was run at a time step increment of 0.2159 s, corresponding to a Courant number of 0.5 (for the progressive wave peak) and  $\theta = 0.5$ . The BFD scheme was run at a time step increment of 0.4317 s, corresponding to a Courant number of 1.0 (for the progressive wave peak) and  $\theta = 0.6$ . The results are presented in Fig. 3 for  $t = 12.95$  s, after the progressive disturbance had travelled exactly 150 m. At this time the exact solution predicted that the peaks, each of depth 4.70 m were located at 140.89 and 430 m, respectively.

As expected from the linear stability analysis, the results shown in Fig. 3 for the BFD scheme illustrate that the peak phase speed is exact for the progressive wave, though the solution is quite dissipative. In contrast, the regressive wave, which effectively ran at a Courant number less than 1 (increased  $N_t$ ), is less damped though subject to phase error (leading disturbances). These results illustrate the difficulty in determining an optimum Courant number, as either phase or amplitude accuracy must be sacrificed in the selection.

The results for the CDG scheme are shown in Fig. 3 for

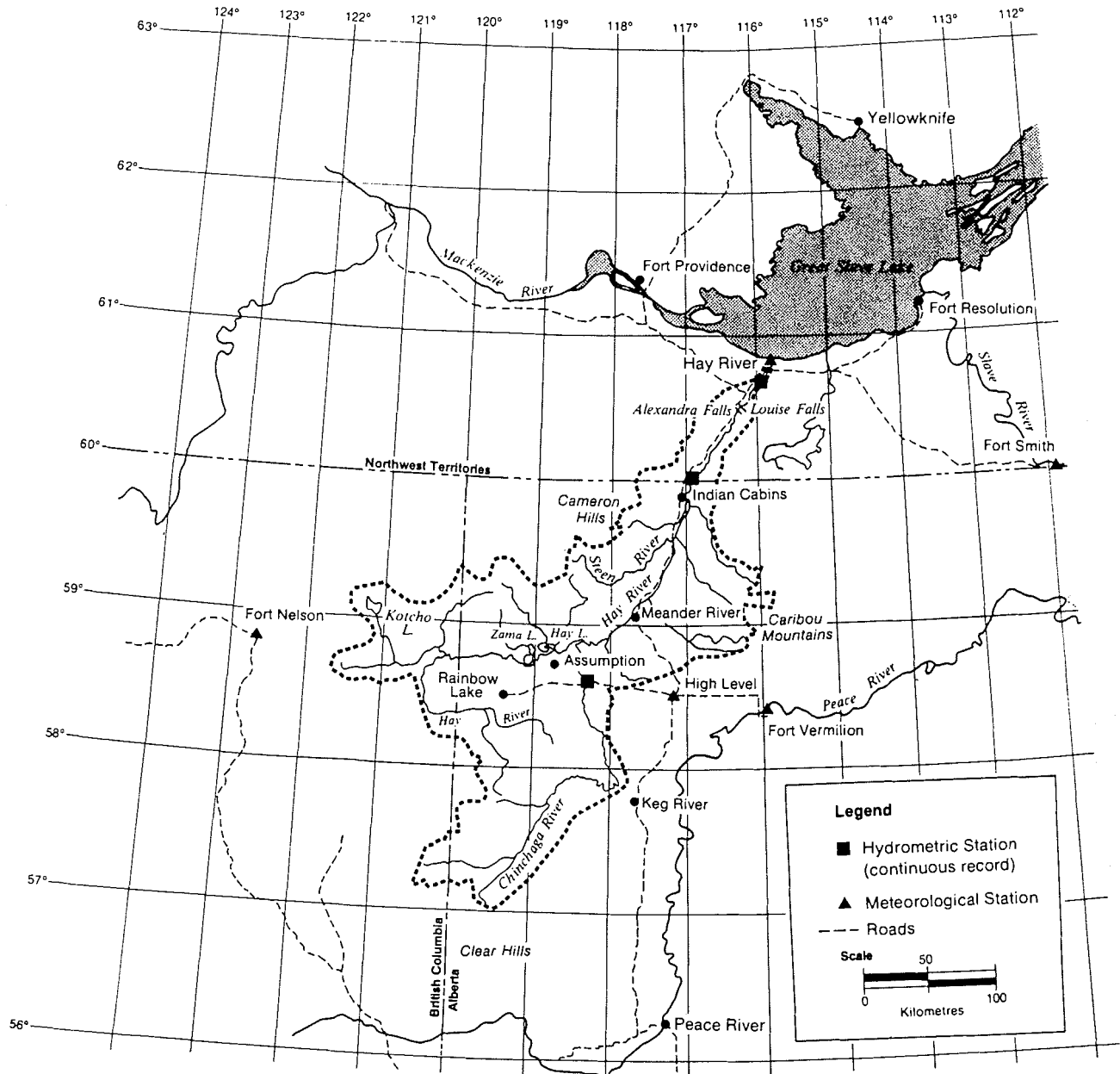


FIG. 4. The Hay River catchment.

both  $\omega = 0.25$  and  $0.50$ , confirming the earlier assertion that the effect of this parameter on phase and amplitude is only marginal. As expected from the linear stability analysis, there is little damping or dispersion of the wave peaks. In addition, comparable accuracy is achieved for both the progressive and regressive waves, illustrating the fact that this scheme is optimum over a range of Courant numbers.

The CDG scheme was found to provide consistently more stable and accurate solutions than either other finite element models or the four-point implicit finite difference scheme, particularly for extremely dynamic events where shocks are present (Hicks and Steffler 1990, 1992). In addition, the ability of CDG scheme to conserve both mass and momentum was established theoretically and in numerical tests (Hicks and Steffler 1990). Implementation of the CDG scheme requires no more data input than standard finite difference methods and, in terms of calibration, requires no parameter variation other than the roughness coefficient.

#### Application to Hay River, N.W.T.

As a practical test of the CDG scheme, it is used to simulate surge propagation on the Hay River. Widely varying geometry, including supercritical and subcritical flow transitions, on this river creates a situation very difficult to simulate accurately using the BFD scheme. Because the town of Hay River, located at the mouth of the Hay River, has suffered severe flooding due to ice jams on numerous occasions, the river has been the object of a series of investigations into the formation and release of ice jams and their effects on water levels at the town (Gerard and Stanley 1988; Gerard *et al.* 1990). Geometric data covering a reach of about 500 km were therefore available for this investigation.

The Hay River originates in the foothills of the Rocky Mountains in northwestern Alberta and flows northeast to Great Slave Lake in the Northwest Territories as shown in Fig. 4. The longitudinal profile of the river is shown in Fig. 5. Upstream of Alexandra Falls the channel is charac-

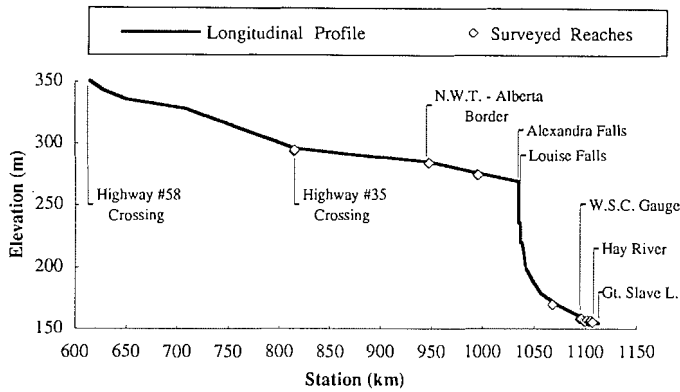


FIG. 5. Longitudinal profile of the Hay River.

terized by widths varying from about 75 to 150 m and slopes from about 1 : 10 000 to 5 : 10 000. Elevation drops of 33 and 15 m occur through Alexandra and Louis Falls, respectively. A sudden narrowing to less than 50 m occurs just downstream of the falls, followed by a gradual increase to 150 m just upstream of the town of Hay River. Bed slopes decrease gradually in this reach from 6 : 10 000 to 2 : 10 000. Further details on the geometry of the river are given by Gerard *et al.* (1990).

Water surface slopes and widths, extending from the Highway 58 crossing of the Chinchaga River (station 615 km) to the town of Hay River (station 1108 km), were determined from 1 : 50 000 scale National Topographic Series (NTS) maps in conjunction with surveyed river cross sections at selected sites. An equivalent rectangular channel was used to define the effective bed elevation at the survey sites by determining average mean depth of the reach based on the 1:2 year return period flood and then subtracting this from the elevation of the geodetic water level for this discharge, as determined from either the measured or a synthesized rating curve for the reach. These bed elevations were then extended throughout the entire domain using the water surface slopes obtained from the NTS maps. Further details of the determination of these values are available in Gerard *et al.* (1990).

Figure 6 illustrates the channel top widths obtained from the NTS maps together with those measured at survey sites. Due to the highly variable nature of these widths, these data were smoothed to obtain an alternate data set for the numerical model. The original and smoothed data sets allowed examination of the effects of rapid width variations shown in Fig. 6 on the model behavior and results.

With the exception of one nonuniform flow reach affected by downstream rapids, the effective hydraulic roughness of the bed,  $k_b$ , was determined for the surveyed reaches for the discharge on the day of the survey. The values of  $k_b$  obtained from the analyses varied from about 0.05 to 0.55 m. These results, plus those deduced for higher discharges from the rating curve for the WSC gauge near Hay River (station 1095.6 km), together with consideration of the nature of the bed material, indicated that a constant value of  $k_b = 0.2$  m would be reasonable for use for this investigation throughout the entire domain.

#### Discretization and boundary conditions

A section spacing of 1 km was used throughout the upstream portion of the study reach. This spacing was consistently decreased, in steps of 15%, to 200 m just upstream

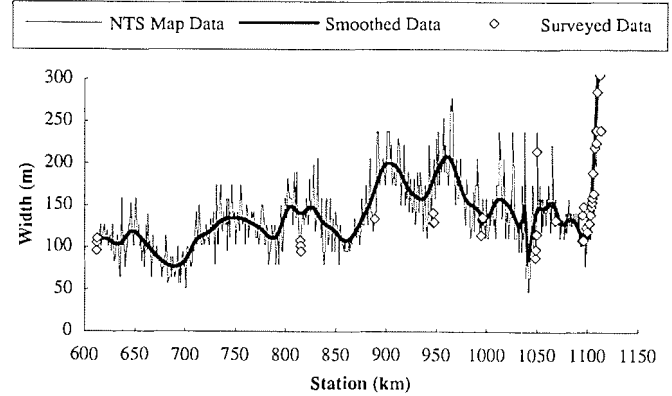


FIG. 6. Hay River channel widths.

of the steep reach in the vicinity of the falls (between stations 1027 and 1032.5 km) and then increased, in steps of 15%, to 500 m further downstream (station 1045 km). A total of 617 cross sections were used in the analysis.

In this investigation, lateral inflows along the study reach were neglected and a constant (carrier) discharge of 500 cm was specified as the initial condition. This discharge is typical of those occurring when ice jams form. Although the study domain encompassed both subcritical and supercritical reaches, the flow remained subcritical at both the upstream and downstream extremities. Therefore, one upstream and one downstream boundary condition were required for the simulation. The upstream boundary condition was taken as the constant carrier discharge, while at the downstream end a constant water level of 156.9 m corresponding to the water level on Great Slave Lake was used.

Steady gradually varied flow profiles were calculated using the CDG model to establish the initial conditions for the unsteady flow simulation. The results of the steady flow analysis, illustrating the subcritical and supercritical transitions, are shown in Fig. 7 for the reach surrounding the falls. The elevation discontinuity at each of the falls was modeled as a steep chute over a single 200 m element.

#### Assumptions for ice jam simulation

Once the gradually varied flow profile was calculated, an ice jam profile was superimposed on the flow. A number of simplifying assumptions concerning the initial jam shape and failure mechanism were used in conducting the unsteady flow analysis. For example, the ice jam was assumed to have a toe length equal to the grid spacing used for the geometric data. The gradually varied (M1) flow profile upstream of the jam was approximated by projecting a horizontal line back from the jam to an intersection with the upstream water level. The flow depth to the phreatic surface within the jam was that for an equilibrium section of a fully developed jam, using the following relationship developed from Pariset *et al.* (1966) (see also Beltaos (1983)):

$$[13] \quad \eta = 0.38\zeta + \frac{5.75}{\mu} \left\{ 1 + \sqrt{1 + 0.07\mu\zeta \left( \frac{k_i}{k} \right)^{1/4}} \right\}$$

where

$$[14] \quad \eta \equiv \frac{d}{S_f b} \quad \text{and} \quad \zeta \equiv \frac{(qk^{1/6}/\sqrt{gS_f})^{3/5}}{S_f b}$$

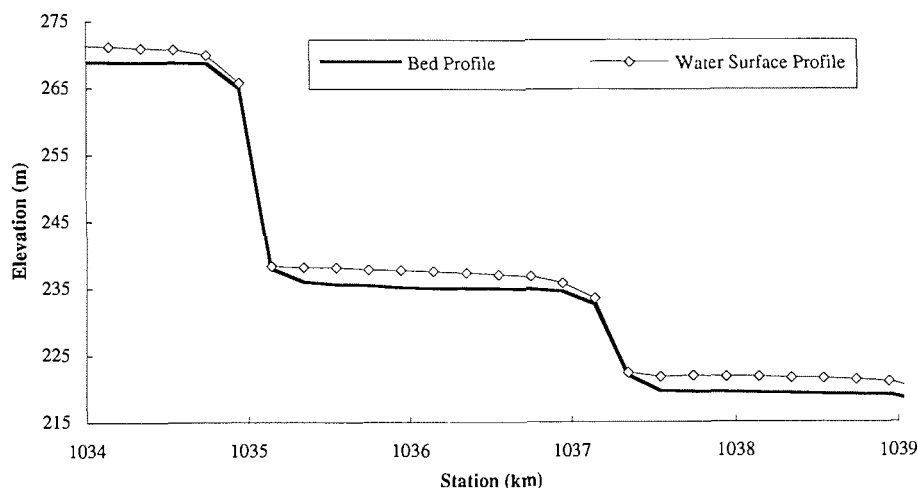


FIG. 7. Steady gradually varied flow profile in the vicinity of the falls (unsmoothed widths).

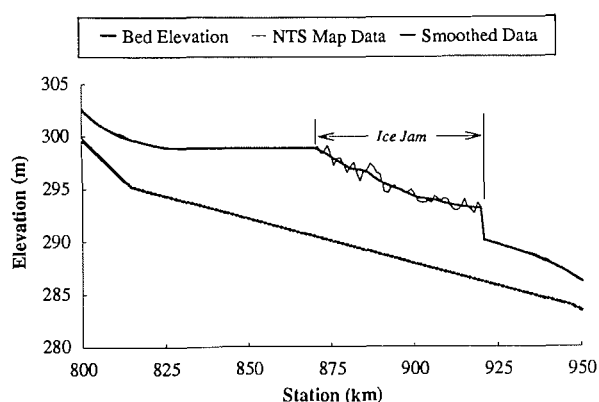


FIG. 8. Initial ice jam profiles based on smoothed and unsmoothed (NTS map) data.

in which  $\mu$  is an internal friction-porosity coefficient,  $d$  is the depth to the phreatic surface,  $q$  is the unit discharge, and  $b$  is the pack width. There were insufficient field data to allow for the determination of  $\mu$ , so for the purpose of this investigation a value of 1.0 was used. Although this is lower than the value of 1.2 suggested by Beltaos (1983), it is midway within the range of values determined for a number of Alberta rivers (Beltaos 1983). This lower value results in slightly larger depths within the ice jam and therefore represents a conservative estimate. The composite roughness,  $k$ , is based on the ice roughness,  $k_i$ , and the bed roughness,  $k_b$ , such that

$$[15] \quad k = \left( \frac{k_i^4 + k_b^4}{2} \right)^{1/4}$$

There are no measurements of the hydraulic roughness of the underside of ice jams for the Hay River. However, estimates based on the surface roughness of in-place ice jams in the East Channel at the town of Hay River in 1987 and 1988, as well as calibration to profiles surveyed through these jams, indicate that a value of  $k_i = 1.1$  m is appropriate (Gerard and Stanley 1988). As a conservative estimate of the characteristics of newly formed jams in the upstream reaches of the Hay River, a constant value of 2 m was used for the roughness of the underside of the ice pack,  $k_i$ , for

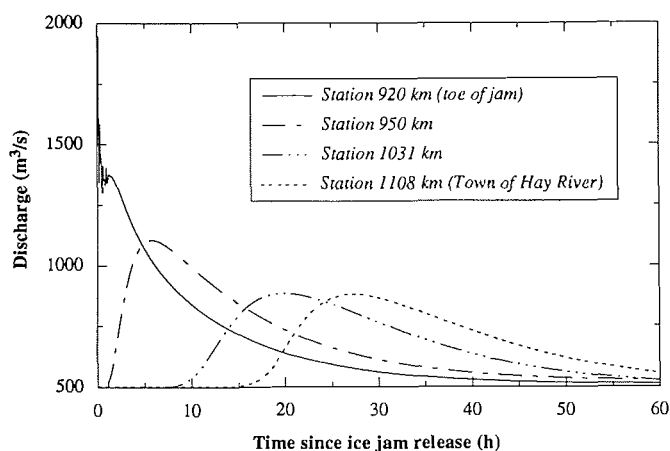


FIG. 9. Hydrographs at stations 920, 950, 1031, and 1108 km (unsmoothed widths).

all runs conducted in this analysis. This value corresponds to a Manning's  $n$  of about 0.045, based on Strickler's equation (Henderson 1966), for the underside of an ice jam.

The release of the ice jam was assumed to be instantaneous along its length, resulting in an acceleration of the stored water over the entire length of the jam. It was also assumed that the ice in the pack followed the water and therefore had no resistance effect on the flow after the time of release. Although these assumptions represent a simplification of the actual physical processes, in the absence of detailed field data on the dynamics of ice jam releases on the Hay River, they do provide an upper bound in terms of the severity of the released wave. Finally, it was assumed that the entire reach downstream of the toe of the jam was open with no ice cover. Additional tests were conducted, in which an ice cover was present downstream of the jam. As might be expected, the resulting wave peaks and speeds were reduced compared to the tests conducted without a downstream ice cover. Details of these results are provided in Gerard *et al.* (1990).

#### Ice jam release simulation

To obtain an indication of the effects of sudden releases on water levels and discharges at the town, a number of ice jam lengths and locations were analyzed for this study

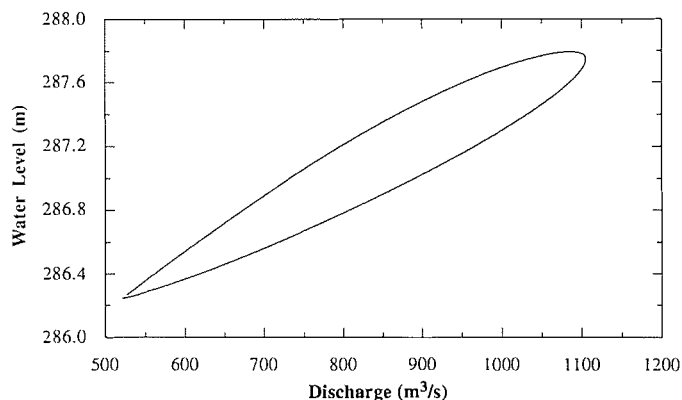


FIG. 10. Rating curve at station 950 km (unsmoothed widths).

(Gerard *et al.* 1990). In this paper, only the results for an ice jam located 190 km upstream of the town at station 920 km are presented. This location was chosen, as it allows a sufficient distance for the initial dynamic surge to transform into an essentially kinematic wave. The jam itself was taken as being 50 km long with the backwater profile extending approximately 40 km further upstream, as shown in Fig. 8. The two jam profiles are for the original and smoothed width data.

Figure 9 illustrates the resulting hydrographs at stations 920 (just downstream of the jam), 950 (close to the toe of the jam), 1031 (just above the falls) and 1108 km (at the town of Hay River), respectively, for the unsmoothed data sets. The fluctuations observed on the hydrograph at station 920 km are associated with the simplified initial ice jam condition and failure process. Results for the smoothed data set were not visually different: the peaks arrived at the downstream locations at almost identical times, with the magnitudes of those peaks only being about 2%–3% higher than those calculated using the varied width data. However, the smoothed data file required fewer iterations per time step (2–3 compared to 3–4). The average propagation speed of about 1.8 m/s is consistent with field observations (Gerard and Stanley 1988).

Figure 10 shows the loop rating curve obtained using the original (unsmoothed widths) at station 950 km, just downstream of the toe of the jam. In contrast to the conditions at this station, the rating curve shown in Fig. 11 for station 1031 km indicates that the wave was approaching a kinematic condition, as almost no looping is evident. The existence of a kinematic condition at this station is supported by the lack of attenuation of the wave peak between this location and the town. Therefore, although the full dynamic equations were being used in the simulation, the CDG scheme successfully modeled this situation in which the friction terms in the equation clearly dominated the acceleration terms.

### Conclusions

As a result of a comprehensive examination of the state of the art in finite element modeling of open channel flow, a new approach called the characteristic-dissipative-Galerkin scheme has recently been developed. This method is able to handle subcritical and supercritical flow transitions; provides stable solutions not only for the extremes of dynamic and kinematic wave conditions, but also through the transi-

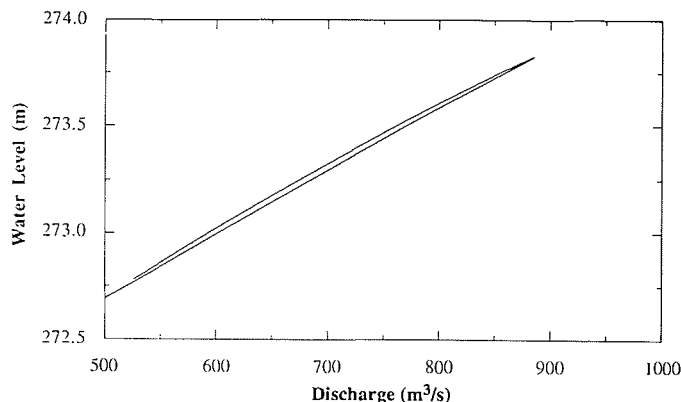


FIG. 11. Rating curve at station 1031 km (unsmoothed widths).

tion between the two; and is markedly more accurate than the more familiar box finite difference scheme. This study illustrates the applicability of the CDG method to practical problems through application of the model to surge propagation on the Hay River, a reach characterized by an extreme range of slopes resulting in supercritical and subcritical transitions. These transitions were captured by the model without special treatment or subdivision by the CDG method. The fact that stable solutions were obtained without adjusting the upwinding parameter means that practical application of the model would only require calibration of physical parameters, *i.e.*, roughness. In addition, implementation of the CDG scheme requires no more data input than the standard finite difference methods.

### Acknowledgements

This research was financially supported through scholarships to the first author from the Natural Sciences and Engineering Research Council of Canada; the Alberta Heritage Scholarship Foundation; the University of Alberta; the North American Life Assurance Co. with the Canadian Council of Professional Engineers; and the Province of Alberta. All are most gratefully acknowledged. The authors would also like to thank Environment Canada and Indian and Northern Affairs Canada, as their support of the ongoing research at Hay River provided the data for the Hay River analysis. Thanks are also extended to Mr. S. Lovell and Mr. M. Jasek for their technical assistances.

- Amien, M. 1968. An implicit method for natural flood routing. *Water Resources Research* 4(4): 719–726.
- Baker, A.J. 1983. *Finite element computational fluid mechanics*. Hemisphere Publishing Corp., New York, N.Y.
- Beltaos, S. 1983. River ice jams: theory, case studies and applications. *ASCE Journal of Hydraulic Engineering* 109: 1338–1359.
- Chow, V.T. 1959. *Open channel hydraulics*. McGraw-Hill Book Company, New York, N.Y.
- Cunge, J.A., Holly, F.M., Jr., and Verwey, A. 1980. *Practical aspects of computational river hydraulics*. Pitman Publishing Company, London, United Kingdom.
- Fread, D.L. 1988. *The NWS DAMBRK model: theoretical background/user documentation*. Office of Hydrology, National Weather Service (NWS), Md.
- Gerard, R., and Stanley, S. 1988. Hay River study phase I — ice jams and flood forecasting. *Water Resources Engineering Report No. 88-6*, Department of Civil Engineering, University of Alberta, Edmonton, Alta.

- Gerard, R., Hicks, F.E., and Jasek, M. 1990. Hay River study phase II — ice jams and flood forecasting. Water Resources Engineering Report No. 90-4, Department of Civil Engineering, University of Alberta, Edmonton, Alta.
- Henderson, F.M. 1966. Open channel flow. MacMillan Publishing Co., Inc., New York, N.Y.
- Hicks, F.E., and Steffler, P.M. 1990. Finite element modeling of open channel flow. Water Resources Engineering Report No. 90-6. Department of Civil Engineering, University of Alberta, Edmonton, Alta.
- Hicks, F.E., and Steffler, P.M. 1992. A characteristic-dissipative-Galerkin scheme for open channel flow. ASCE Journal of Hydraulic Engineering. **118**: 337-352
- Hughes, T.J.R., and Mallet, M. 1986. A new finite element formulation for computational fluid dynamics: III. The generalized streamline operator for multidimensional advective-diffusive systems. Computer Methods in Applied Mechanics and Engineering. **58**: 305-328.
- Katopodes, N.D. 1984. A dissipative Galerkin scheme for open-channel flow. ASCE Journal of Hydraulic Engineering **110(HY4)**: 450-466.
- Keulegan, G.B. 1938. Laws of turbulence in open channels. Journal of Research of the National Bureau of Standards, U.S. Department of Commerce, **21**: 707-741.
- Pariset, E., Hausser, R., and Gagnon, A. 1966. Formation of ice covers and ice jams in rivers. ASCE Journal of Hydraulic Engineering, **92**: 1-24.
- Schlichting, H. 1979. Boundary layer theory. 7 ed. McGraw-Hill Book Company, New York, N.Y.
- White, F.M. 1986. Fluid mechanics. 2 ed. McGraw-Hill Book Company, New York, N.Y.

#### List of symbols

$A$	channel cross-sectional area perpendicular to the flow	$\mathbf{A}$	convection matrix
		$B$	channel width (and ice pack width)
		$c$	celerity
		$C$	Courant number
		$C_*$	non-dimensional Chezy coefficient
		$d$	depth to the phreatic surface
		$F$	flux vector
		$f_c, f_n$	source term in conservation and non-conservation equations, respectively
		$g$	acceleration due to gravity
		$H$	depth of flow
		$k_b, k_i, k$	effective bed, ice, and composite roughness heights, respectively
		$K$	constant in the log-law velocity equation
		$n$	Manning coefficient
		$P$	wetted perimeter
		$q$	discharge per unit width of channel
		$Q$	discharge
		$R$	hydraulic radius
		$S_f$	friction slope
		$S_0$	bed slope
		$t$	time coordinate
		$U$	cross-sectionally averaged longitudinal velocity
		$x$	longitudinal coordinate
		$\phi$	vector of unknowns
		$\eta$	non-dimensional depth to the phreatic surface at an equilibrium section of a fully developed ice jam
		$\theta$	implicitness
		$\mu$	ice jam internal friction-porosity coefficient
		$\omega$	upwinding coefficient